JOURNAL OF COMPUTATIONAL PHYSICS 4, 67–96 (1969)

A Method for Calculating Frontal Motion I. One Dimensional Tests

Z. S. ALTERMAN[1] AND E. ISAACSON

Courant Institute of Mathematical Sciences, New York University, New York, New York 10012[2]

Received July 19, 1968

ABSTRACT

A method is developed for treating the motion of a cold front in a simplified model having a single space dimension. With this method it is not necessary to follow the "particles" at the front, hence the programming of the numerical scheme is simpler than in previous methods. Calculations of "equilibrium" state and motion of the front due to inflow of cold air at the north proved numerically stable through prolonged periods both for a single layer model and for a two layer model. The "equilibrium" solutions for both models are similar. The time dependent solutions for these models show qualitative agreement in the motion of the front and in the velocity distribution. However, the solutions for the two models differ quantitively.

INTRODUCTION

This paper develops a simple method for calculating the motion of a cold front in a single space dimension. The new feature of the method involves initially "inserting" a very shallow layer of cold air over that portion of the ground which is covered by warm air. With this technique it is not necessary, as it was in a previous paper by Kasahara, Isaacson and Stoker ([3], [4]), to devise a special scheme to follow the "particles" at the front-hence the programming of the calculations is indeed simpler. Furthermore, it may prove to be possible to extend the method to treat the full two-dimensional model. In this event it should be possible to compute

[1] Presently at the Department of Environmental Sciences, Tel-Aviv University, Tel-Aviv, Israel.

[2] The authors gratefully acknowledge the personal encouragement and scientific advice given generously by J. J. Stoker. The research reported in this paper was supported by a Ford Foundation Grant to the first author and was supported under contract AT(30-1)-1480 with the U.S. Atomic Energy Commission. Reproduction in whole or in part is permitted for any purpose of the United States Government.

well into the occlusion phase more readily than it could be done by the method of [3]. (In the one-dimensional model, the Coriolis force remains constant, hence the results may only have physical significance for a short time—the principal reason for making these calculations is to verify that we can safely avoid following the frontal particles. In Section 7, we give another application of this method by computing the river flood that results from breaking a dam.)

The initial state of the dynamical system consists of a cold wedge of air at the ground with a warm layer over it. Fig. 1 shows the wedge pointing from north to

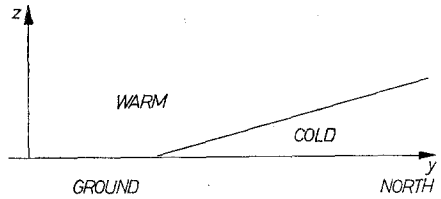

FIG. 1. Vertical cross section of the wedge of cold air.

south (in the negative y-direction). Initially the velocity in both layers is constant and in the direction of the x-axis (to be thought of as the eastward direction). To make the problem one dimensional, we neglect the x-dependence of all quantities involved. The fluid in each layer is assumed to be a perfect incompressible fluid with constant density subject to gravity.

1. EQUATIONS

Upon following the notation of [3] neglecting x-dependence, and adding resistance terms R and R' the equations of motion become

$$v_t + vv_y = -g\left[\frac{\rho'}{\rho} h'_y + \left(1 - \frac{\rho'}{\rho}\right) h_y\right] - fu + R \tag{1}$$

$$v'_t + v'v'_y = -gh'_y - fu' + R' \tag{2}$$

and the equations of continuity are

$$h_t + vh_y + hv_y = 0 \tag{3}$$

$$(h' - h)_t + v'(h' - h)_y + (h' - h)\, v'_y = 0. \tag{4}$$

In the lower layer (cold air) ρ represents the density, h the height of the upper surface of the layer, and u and v represent eastward and northward velocity

components. The corresponding quantities in the upper layer are distinguished with primes. The x-components of velocity u and u' are assumed to be constants. R and R' are the y-components of the friction acting on the two layers. We shall solve these equations with appropriate initial and boundary conditions. We first consider the simpler set of equations obtained by an approximate treatment that cuts the number of dependent variables in half by simply neglecting the dynamics of the perturbations in the warm air layer. (On this assumption, numerical solutions for a two space dimensional model have been given in [3]). Hence, for a single layer model, in one space dimension and with the inclusion of a frictional resistance term, we have

$$v_t + vv_y + g\left(1 - \frac{\rho'}{\rho}\right) h_y = f\left(\frac{\rho'}{\rho} u' - u\right) + R \tag{5}$$

$$h_t + hv_y + vh_y = 0. \tag{6}$$

The friction term in Eqs. (1), (2) and (5) is taken proportional to the square of the y-component of the velocity. A more detailed description of the friction term follows later.

The system of partial differential equations (1)–(4) has an exact solution, corresponding to a stationary front

$$v' = 0 \tag{7}$$

$$h'_y = -\frac{f}{g} u' \tag{8}$$

$$v = 0 \tag{9}$$

$$h_y = \frac{f}{g(1 - \rho'/\rho)} \left(\frac{\rho'}{\rho} u' - u\right). \tag{10}$$

The stationary solution for Eqs. (5) and (6) is given by (9) and (10) alone. Eqs. (8) and (10) show that the slope of the surface of both the warm and the cold air is constant in this stationary solution. This solution corresponds to the configuration of a wedge of cold air in a region which does not include the intersection of the wedge surface with the earth—i.e. the front. As pointed out in [3] a special numerical difficulty arises from the fact that the front is a free boundary along which the differential equations are in a sense singular. The main purpose of this study is to find a numerical method, for determining the motion of the front, without the labor of following the front from one time step to another. To this end, wherever at time $t = 0$ there is no cold air on the ground, we insert a quite thin layer of cold air. Hopefully this device will be useful in the numerical solution of the front problem for two space dimensions.

2. Initial Conditions

At the time $t = 0$: the front of the cold air layer is located at $y = y_c$; within the region $0 < y < Y$ the surface of the layer has constant slope for $y_c < y < Y$ and is at a given constant level for $0 < y < y_c$. Fig. 2 shows the shallow layer of

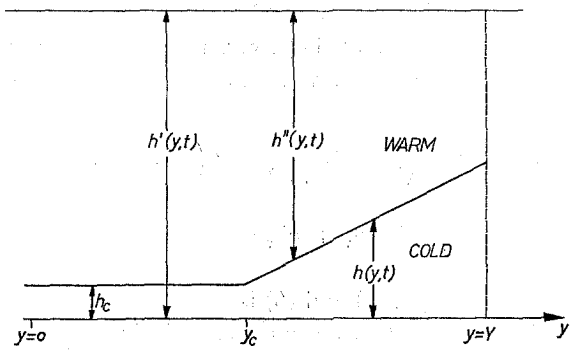

Fig. 2. Vertical cross section of the two air layers.

cold air in front of the wedge. By choosing the slope of the wedge to be equal to the slope in the stationary solution, the initial conditions for Eqs. (1)–(4) become

$$v' = 0 \tag{11}$$

$$h'' = h''_y(y - y_c) + h''_c \tag{12}$$

$$h''_y = \begin{cases} \dfrac{f}{g(1 - \rho'/\rho)}(u - u') & y_c \leqslant y \leqslant Y \\ -\dfrac{f}{g}u' & 0 \leqslant y < y_c \end{cases} \tag{13}$$

$$v = 0 \tag{14}$$

$$h = h_y(y - y_c) + h_c \tag{15}$$

$$h_y = \begin{cases} \dfrac{f}{g(1 - \rho'/\rho)}\left(\dfrac{\rho'}{\rho}u' - u\right) & y_c \leqslant y \leqslant Y \\ 0 & 0 \leqslant y < y_c \end{cases} \tag{16}$$

here $h'' = h' - h$ denotes the depth of the warm air above the surface of the cold air and h''_c and h_c are constants having the values of h'' and h respectively at $y = y_c$. The initial conditions for Eqs. (5) and (6) are given by (14)–(16) alone.

These initial conditions do not in general constitute a steady state solution. For example, on neglecting resistance, we find an initial acceleration in the shallow layer of cold air. That is, in this layer at the initial time,

$$v_t = f\left(\frac{\rho'}{\rho}u' - u\right) = \text{const} \neq 0 \qquad \text{for} \quad 0 \leqslant y \leqslant y_c \tag{17}$$

(unless $(\rho'/\rho)u' = u$).

3. Boundary Conditions

The point $y = 0$ is assumed to be far enough from the cold front so that boundary conditions here do not influence the front. The only condition to be satisfied, is that no additional disturbance should propagate from $y = 0$ into the region $0 \leqslant y \leqslant Y$. At $y = Y$ conditions can be prescribed in a variety of ways, depending on the physical conditions assumed to hold there. We considered the following cases:

(a) $v(Y, t)$ and $h(Y, t)$ determined by extrapolation from $y \leqslant Y$.

(b) Same as in (a), if $v(Y, t + \Delta t) \geqslant 0$; otherwise set $v(Y, t + \Delta t) = 0$.

(c) Inflow of cold air into the wedge either periodically varying in time (with period T), or increasing to a constant flow velocity.

$$v(Y, t) = V_p\left[\cos\frac{2\pi t}{T} - 1\right] \qquad t \geqslant 0 \tag{18}$$

or

$$v(Y, t) = \begin{cases} V_p\left[\cos\dfrac{2\pi t}{T} - 1\right] & 0 \leqslant t \leqslant \frac{1}{2}T \\ -2V_p & \frac{1}{2}T \leqslant t \end{cases} \tag{19}$$

4. The Resistance Term

The resistance terms in Eqs. (1), (2) and (5) are similar to the hydraulic resistance for flow in a channel. They account mainly for the slowing down of the flow in the shallow layer of cold air to the south of the cold front. In Eq. (1), for the cold air, we take

$$R = \alpha\frac{v\,|\,v\,|}{hh''} \tag{20}$$

and in Eq. (2) for the warm air

$$R' = \frac{\rho'}{\rho}\alpha\frac{v'\,|\,v'\,|}{hh''}. \tag{21}$$

In the single layer case, Eqs. (5) and (6), when h'' and v' do not occur explicitly, h'' in Eq. (20) is absorbed into the coefficient, and the resistance term in Eq. (5) is written as

$$R = \alpha \frac{v \mid v \mid}{h}. \tag{22}$$

The right hand side of Eq. (22) is the same as the Chézy formula for the hydraulic resistance for flow in a channel [7]. Mintz [5] assumes the horizontal frictional force to depend on the vertical stress, and takes it specifically at the surface of the earth to be proportional to $v \mid v \mid$, as did Phillips [6]. Now the y-component of the three dimensional equations of motion includes the term $(1/\rho)(\partial\tau_y/\partial p)$. Here τ_y is the y-component of the frictional stress acting across a horizontal surface and p stands for pressure. The factor $1/h$ in (22) enters through an approximation to the p-derivative, since the hydrostatic assumption implies that Δp, the change in pressure from the top to the bottom of the cold air layer, is proportional to h.

5. Dimensionless Variables

The following new dimensionless variables are introduced in the case of the two layered model, Eqs. (1)–(4), (11)–(16) and (20)–(21)

$$\begin{aligned} &\tau = t/\Delta t \quad \eta = y/\Delta s \quad \lambda = \Delta t/\Delta s \\ &\hat{v} = \lambda v \quad \hat{v}' = \lambda v' \quad \hat{h} = \lambda^2 g h \quad \hat{h}'' = \lambda^2 g h''. \end{aligned} \tag{23}$$

Δt and Δs denote units for time and length with ratio λ, a suitably determined constant. Also we define the following new parameters:

$$\begin{aligned} &G = fu\Delta t\lambda \qquad G' = fu'\Delta t\lambda \\ &P = \alpha\Delta s\lambda^4 g^2 \qquad P' = \sigma P \qquad \sigma = \rho'/\rho. \end{aligned} \tag{24}$$

With the aid of (23) and (24), Eqs. (1)–(4) could be written in dimensionless form. But we find it convenient to further simplify the equations. We now drop the circumflex and use v to represent the dimensionless velocity, $\hat{v}$, in the lower layer, in addition we introduce new variables w, ϕ and ψ by

$$v = \hat{v} \qquad w = \hat{v}' \qquad \phi = 2\sqrt{\hat{h}} \qquad \psi = 2\sqrt{\hat{h}''} \tag{25}$$

Equations (1)–(4) then become

$$v_\tau + vv_\eta + \tfrac{1}{2}\sigma\psi\psi_\eta + \tfrac{1}{2}\phi\phi_\eta = -G + 16P\frac{v\,|\,v\,|}{\phi^2\psi^2} \tag{26}$$

$$w_\tau + ww_\eta + \tfrac{1}{2}\psi\psi_\eta + \tfrac{1}{2}\phi\phi_\eta = -G' + 16P'\frac{w\,|\,w\,|}{\phi^2\psi^2} \tag{27}$$

$$\phi_\tau + v\phi_\eta + \tfrac{1}{2}\phi v_\eta = 0 \tag{28}$$

$$\psi_\tau + w\psi_\eta + \tfrac{1}{2}\psi w_\eta = 0. \tag{29}$$

The initial conditions are rewritten as

$$\begin{aligned} w &= 0 \\ \psi &= 2[h''_\eta(\eta - \eta_c) + h''_c]^{1/2} \\ v &= 0 \\ \phi &= 2[\hat{h}_\eta(\eta - \eta_c) + \hat{h}_c]^{1/2} \end{aligned} \tag{30}$$

at $t = 0$, $0 \leqslant \eta \leqslant Y/\Delta s$.

The dimensionless variables in the case of the equations for a single layer, are defined in a slightly different fashion. τ, η, λ and $\hat{v}$ are defined as in Eq. (23). $\hat{h}$, G, P will now be defined in the following way

$$\hat{h} = g\left(1 - \frac{\rho'}{\rho}\right)\lambda^2 h \tag{31}$$

$$G = f\Delta t\lambda\left(\frac{\rho'}{\rho}u' - u\right) \tag{32}$$

$$P = \alpha\Delta t\lambda g\left(1 - \frac{\rho'}{\rho}\right). \tag{33}$$

By introducing $\phi = 2\sqrt{\hat{h}}$ and omitting the circumflex symbols, i.e. setting $v = \hat{v}$, Eqs. (5) and (6) for the single layer become

$$v_\tau + vv_\eta + \tfrac{1}{2}\phi\phi_\eta = G + 4P\frac{v\,|\,v\,|}{\phi^2} \tag{34}$$

$$\phi_\eta + \tfrac{1}{2}\phi v_\eta + v\phi_\eta = 0. \tag{35}$$

The initial conditions (14)–(16) become here

$$\begin{aligned} v &= 0 \\ \left(\frac{\phi}{2}\right)^2 &= \left(\frac{\phi_c}{2}\right)^2 + G(\eta - \eta_c) \qquad \eta_c \leqslant \eta \leqslant Y/\Delta s \\ \phi &= \phi_c \qquad\qquad\qquad\qquad 0 \leqslant \eta \leqslant \eta_c\,, \end{aligned} \tag{36}$$

where $\eta_c = y_c/\Delta s$ and $\phi_c = 2\lambda\sqrt{gh_c}$.

6. Difference Equations

The finite difference scheme chosen is similar to the scheme used in [3]. The grid intervals in the y direction are chosen to be equal to Δs, the time-increments equal Δt, so that the increments $\Delta\eta$, and $\Delta\tau$ in η and τ are unity. (The finite difference scheme is accurate to terms of second order and we will retain the symbol $\Delta\tau$ in some of the subsequent formulae in order to make this fact transparent.)

The difference equations are obtained by first replacing time derivatives by first order centered differences, e.g.

$$[v(\eta,\tau+\Delta\tau)-v(\eta,\tau)]/\Delta\tau \equiv v(\eta,\tau+1)-v(\eta,\tau) \cong v_\tau(\eta,\tau+\tfrac{1}{2}), \tag{37}$$

a formula which is accurate to second order in $\Delta\tau$. All space derivatives occur multiplied by one of the dependent variables. The space derivatives are to be approximated at time $\tau+\frac{1}{2}$ and the variable factor is replaced by the arithmetic mean of its values at τ and $\tau+1$. With the notation

$$\langle v\rangle = \tfrac{1}{2}[v(\eta,\tau+1)+v(\eta,\tau)], \tag{38}$$

the difference equations for (26)–(29) may be derived by first setting

$$\begin{aligned}
&v(\eta,\tau+\Delta\tau)\\
&\quad= v(\eta,\tau) - G\Delta\tau + 16P\langle v\rangle\left[\frac{|v|}{\phi^2\psi^2}\right]_{\tau+\frac{1}{2}\Delta\tau}\Delta\tau - \Delta\tau\left[\langle v\rangle\frac{\partial v}{\partial\eta}\left(\eta,\tau+\frac{1}{2}\Delta\tau\right)\right.\\
&\qquad\left.+\frac{1}{2}\sigma\langle\psi\rangle\frac{\partial\psi}{\partial\eta}\left(\eta,\tau+\frac{1}{2}\Delta\tau\right)+\frac{1}{2}\langle\phi\rangle\frac{\partial\phi}{\partial\eta}\left(\eta,\tau+\frac{1}{2}\Delta\tau\right)\right]\\
&w(\eta,\tau+\Delta\tau)\\
&\quad= w(\eta,\tau) - G'\Delta\tau + 16P'\langle w\rangle\left[\frac{|w|}{\phi^2\psi^2}\right]_{\tau+\frac{1}{2}\Delta\tau}\Delta\tau - \Delta\tau\left[\langle w\rangle\frac{\partial w}{\partial\eta}\left(\eta,\tau+\frac{1}{2}\Delta\tau\right)\right.\\
&\qquad\left.+\frac{1}{2}\langle\psi\rangle\frac{\partial\psi}{\partial\eta}\left(\eta,\tau+\frac{1}{2}\Delta\tau\right)+\frac{1}{2}\langle\phi\rangle\frac{\partial\phi}{\partial\eta}\left(\eta,\tau+\frac{1}{2}\Delta\tau\right)\right]\\
&\phi(\eta,\tau+\Delta\tau)\\
&\quad= \phi(\eta,\tau) - \Delta\tau\left[\langle v\rangle\frac{\partial\phi}{\partial\eta}\left(\eta,\tau+\frac{1}{2}\Delta\tau\right)+\frac{1}{2}\langle\phi\rangle\frac{\partial v}{\partial\eta}\left(\eta,\tau+\frac{1}{2}\Delta\tau\right)\right]\\
&\psi(\eta,\tau+\Delta\tau)\\
&\quad= \psi(\eta,\tau) - \Delta\tau\left[\langle w\rangle\frac{\partial\psi}{\partial\eta}\left(\eta,\tau+\frac{1}{2}\Delta\tau\right)+\frac{1}{2}\langle\psi\rangle\frac{\partial w}{\partial\eta}\left(\eta,\tau+\frac{1}{2}\Delta\tau\right)\right].
\end{aligned} \tag{39}$$

The quantities that are to be evaluated at $(\eta,\tau+\frac{1}{2}\Delta\tau)$, are expressed in terms of their Taylor series expansions about (η,τ) up to terms of first order in $\Delta\tau$ which

ensures that (39) is correct to second order in $\Delta\tau$. The first order time derivatives occurring in these Taylor series are then replaced by space derivatives through the use of the differential equations. All space derivatives are then approximated by centered differences. The result is a set of four linear equations in v, w, ϕ and ψ at the point η and at the time $\tau + \Delta\tau$, namely

$$F_1\phi^{\tau+1} + F_2 v^{\tau+1} = F_3 \tag{40}$$

$$F_4\psi^{\tau+1} + F_5 w^{\tau+1} = F_6 \tag{41}$$

$$F_7 v^{\tau+1} + F_8\phi^{\tau+1} + F_9\psi^{\tau+1} = F_{10} \tag{42}$$

$$F_{11} w^{\tau+1} + F_{12}\phi^{\tau+1} + F_{13}\psi^{\tau+1} = F_{14} \tag{43}$$

here the coefficients are

$$F_1 = 1 + \tfrac{1}{4}v^{\tau+1/2} \qquad F_2 = \tfrac{1}{2}\phi^{\tau+1/2}$$

$$F_3 = \phi^\tau - \tfrac{1}{2}v^\tau\phi_\eta^{\tau+1/2} - \tfrac{1}{4}\phi^\tau v_\eta^{\tau+1/2}$$

$$F_4 = 1 + \tfrac{1}{4}w_\eta^{\tau+1/2} \qquad F_5 = \tfrac{1}{2}\psi_\eta^{\tau+1/2}$$

$$F_7 = 1 + \frac{1}{2}v_\eta^{\tau+1/2} - 8P\left[\frac{|v|}{\phi^2\psi^2}\right]^{\tau+1/2}$$

$$F_8 = \tfrac{1}{4}\phi_\eta^{\tau+1/2} \qquad F_9 = \tfrac{1}{4}\sigma\psi_\eta^{\tau+1/2}$$

$$F_{10} = v^\tau\left(1 - \frac{1}{2}v_\eta^{\tau+1/2} + 8P\left[\frac{|v|}{\phi^2\psi^2}\right]^{\tau+1/2}\right) - G - \frac{1}{4}\sigma\psi^\tau\psi_\eta^{\tau+1/2} - \frac{1}{4}\phi^\tau\phi_\eta^{\tau+1/2}$$

$$F_{11} = 1 + \frac{1}{2}w_\eta^{\tau+1/2} - 8P'\left[\frac{|w|}{\phi^2\psi^2}\right]^{\tau+1/2}$$

$$F_{12} = \tfrac{1}{4}\phi_\eta^{\tau+1/2} \qquad F_{13} = \tfrac{1}{4}\psi_\eta^{\tau+1/2}$$

$$F_{14} = w^\tau\left(1 - \frac{1}{2}w_\eta^{\tau+1/2} + 8P'\left[\frac{|w|}{\phi^2\psi^2}\right]^{\tau+1/2}\right) - \frac{1}{4}\psi^\tau\psi_\eta^{\tau+1/2} - \frac{1}{4}\phi^\tau\phi_\eta^{\tau+1/2} - G'. \tag{44}$$

Equations (40)–(43) are then solved, and the functions at the time $\tau + 1$ are obtained explicitly in terms of the known values of the functions at the time τ.

The finite difference approximations to the equations for the single layer model are obtained in a similar fashion.

7. Waves in Sloping Channels

In order to check the numerical procedure for solving the frontal motion problem, we obtained the solution of a simple problem governed formally by the same equations and treated by a different method in [2].

The equations of motion and continuity for unsteady nonlinear waves in a sloping channel, with hydraulic resistance are

$$v_t + vv_y + gh_y + \frac{kv \mid v \mid}{h} = gm \tag{45}$$

$$h_t + vh_y + hv_y = 0 \tag{46}$$

with depth h, particle velocity v, distance along the channel y, coefficient of resistance k,[3] and slope of the channel $-m$. Dressler [1] considered the problem without friction and Whitham [8] gave an expansion for the solution without slope.

As an illustrative example, we consider the specific unsteady reservoir discharge problem with initial conditions shown in Fig. 3. The triangular wedge of water in the reservoir is initially at rest ($v = 0$) with a horizontal surface and depth H at the y-coordinate where the dam is located. The dam is removed at time $t = 0$.

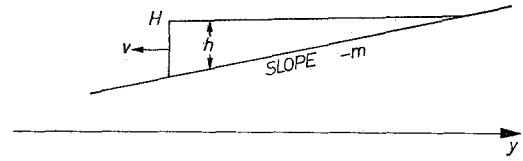

FIG. 3. The initial state of a reservoir on sloping ground.

This is the dam break problem for the case of no water in front of the dam. Its solution will be obtained numerically as a limiting case of the dam break problem *with* water in front of the dam. We first treated cases where the slope is zero and later solved a problem with a sloping channel.

The difference equations which we had described for solving equations (5) and (6) are now applied to Eqs. (45) and (46) with $\Delta y = \Delta s = 5000$ ft, $\lambda = \Delta t/\Delta s = .0024$ sec/ft, $k = 0$, $m = 0$, and $g = 32.15$ ft/sec^2. Fig. 4 shows the well known solution (e.g. see [7]) in the case of a small horizontal layer of water in front of the suddenly removed dam. In this and the subsequent calculations, the dam is placed at $y = 100$ units and its location is indicated by the arrowhead (one unit is 10^4 feet). The initial depth of water in the reservoir is $H = 250$ feet, the depth of water

[3] Note that we have used the symbol α for the resistance coefficient for air.

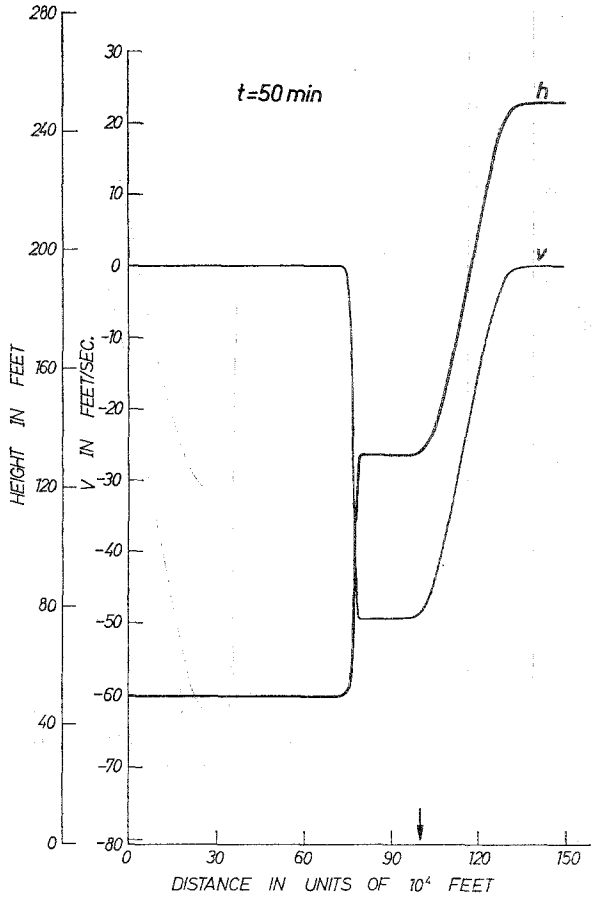

FIG. 4. Height h and velocity v of water, 50 minutes after dam break. $h_c = 50$ feet.

in front of the dam is $h_c = 50$ feet. Fig. 4 shows the distribution of h and v after 50 minutes. Fig. 5 shows the solution after 50 minutes for the problem where initially $H - h_c = 200$ feet, but $h_c = 10$ feet. The hydraulic jump (bore) at the front of the moving water is, as expected, smaller than in Fig. 4. Theoretically, the discontinuity in h should decrease to zero for h_c decreasing to zero. However, it is found experimentally that for a given grid spacing Δy, the jump in h does not decrease below a certain value $h_{\Delta y}$. In other words, for a given grid size, the numerical results are significant only if h_c is not too small.

In order to overcome this difficulty, we simply treated the region in which $h < h_{\Delta y}$ as one in which the velocity is set equal to what it is at the place where $h = h_{\Delta y}$

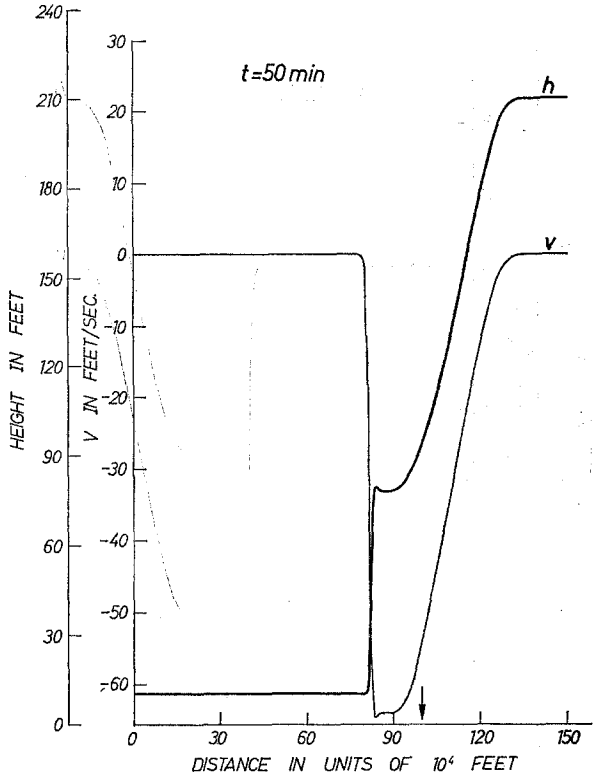

FIG. 5. Height h and velocity v of water, 50 minutes after dam break. $h_c = 10$ feet.

(a simple extrapolation). Fig. 6 shows the solution after 60 minutes when initially $H - h_c = 200$ ft and $h_c = 10^{-6}$ ft. The limiting depth for extrapolation of velocity was $h_{\Delta y} = .01H = 2$ ft. The solution shown in Fig. 6 agrees with the expected result (e.g. see [7]) for flow into a dry channel.

The same method of solution was then applied while taking hydraulic resistance into account. Fig. 7 shows the result for a resistence coefficient of $k = 0.0108$, $h_c = 1$ ft and H, $h_{\Delta y}$, λ unchanged from the values used in the example for Fig. 6. The depth $h(y, t)$ has now the shape calculated and drawn by Whitham [8] for the tongue of the progressing fluid.

The numerical results were checked by doing many calculations of the same problem for varying values of Δy with and without changing the value of λ. The dependence on the specific finite difference scheme was also checked by using a simple first order scheme for several space intervals, Δy, near the front of the wave. The results did not change appreciably.

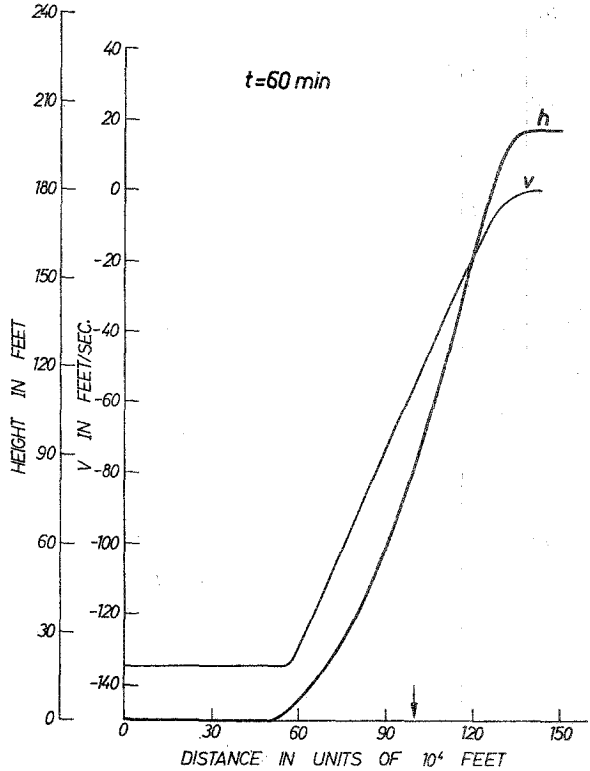

FIG. 6. Height h and velocity v of water, 60 minutes after dam break. No water in front of dam initially.

In order to avoid the spurious oscillations which tend to appear at discontinuities, simple space averaging was performed every few time steps. That is, the velocity and height were smoothed by adding respectively to $v(y, t)$ and to $h(y, t)$ the terms

$$f_{\text{dis}}[v(y + \Delta y, t) - 2v(y, t) + v(y - \Delta y, t)]$$

and (47)

$$f_{\text{dis}}[h(y + \Delta y, t) - 2h(y, t) + h(y - \Delta y, t)].$$

After numerical experimentation we selected $f_{\text{dis}} = .1$. The use of (47) after every forty time steps made it possible to proceed with the computation for a long time, even though somewhat smaller oscillations still developed near the bore. But, using (47) after every ten steps or more often, produced quite smooth results. In all of our calculations for figures 4–8 the smoothing formula was used after every 8 to 40 time steps.

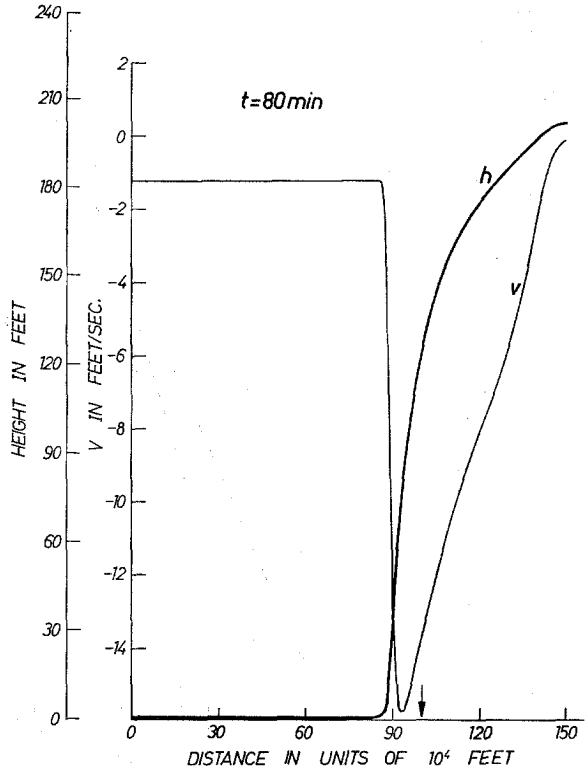

FIG. 7. Effect of hydraulic resistance ($\alpha = -0.01$) on height h and velocity v of water, 80 minutes after dam break. No water in front of the dam initially.

We finally treated a case where the bottom had a gentle slope. Fig. 8 shows the solution in a sloping channel at the time $t = 70$ min. The slope is $m = 0.0001$, $h_c = 10^{-6}$ ft, and the depth $H - h_c = 200$ ft just above the dam, initially. The program worked without any further change. The depth of water decreases linearly behind the dam at the initial instant. The upper portion of the reservoir still shows this effect after 70 minutes since the rarefaction wave hasn't reached the upstream end of the pool.

8. Results for the Single Layer Model of Frontal Motion

After experimenting with the numerical scheme on the dam break problem, we then applied the same method to the single layer model of frontal motion. The following values of the parameters were chosen in the cases we next describe:

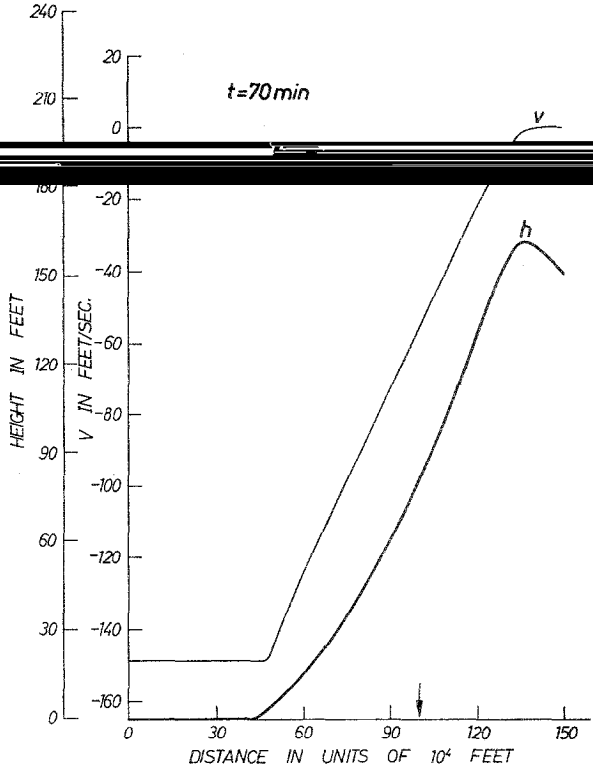

FIG. 8. 70 minutes after dam break in a sloping channel. h is the depth of water above the sloping ground.

$$\Delta s = 5.10^4 \text{ ft}$$
$$\Delta t = 120 \text{ sec}$$
$$\lambda = .0024 \text{ sec/ft}$$
$$Y = 300\Delta s$$
$$y_0 = 200\Delta s$$
$$g = 32.1521 \text{ ft/sec}^2$$
$$f = 10^{-4} \text{ sec}^{-1}$$
$$u = 10 \text{ ft/sec}$$
$$\frac{\rho'}{\rho} u' = 50 \text{ ft/sec}$$
$$g\left(1 - \frac{\rho'}{\rho}\right) = 0.6 \text{ ft/sec}^2$$

As explained earlier we used the smoothing formulae (47) regularly (with a fixed frequency in each case ranging from 8–40 time steps).

a. "STATIONARY" STATE

We first computed with the initial conditions (14)–(16) and the boundary condition of no inflow of cold air from the north. These produced stable, essentially stationary results for various values of h_c, $10^{-8} \leqslant h_c \leqslant 1$ (in feet) and for various values of the resistance coefficient $-10^{-2} \leqslant \alpha \leqslant 0$. By "essentially stationary" we mean that the variation of $h(y, t)$ in time is negligible. That is, for $0 \leqslant t \leqslant 1000$ min, we found the phase lag $p(y, t)$, defined by $h(y, t) = h(y + p(y, t), 0)$, satisfied

$$|p(y, t)| < 3\Delta s \qquad \text{for} \quad |y - y_c| < 10\Delta s,$$

while

$$|p(y, t)| < \Delta s \qquad \text{for} \quad |y - y_c| > 10\Delta s$$

From Eq. (17), we expect $v(y, t)$ to increase in time. The increase is slowed down by the hydraulic resistance throughout the region $0 \leqslant y < y_c$. However v is not constant for a given time. There is an increase in velocity near y_c. Fig. 9 shows the results after 1000 minutes, when we used $h_c = .1$ and $\alpha = -.0001$. The height h of

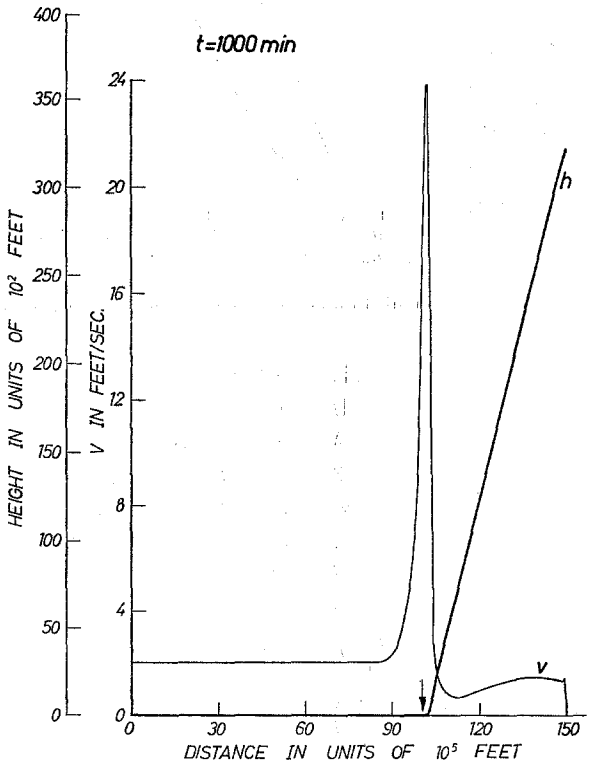

FIG. 9. "Stationary" state after 1000 minutes. The arrow indicates the initial location of the front.

the cold layer has not changed appreciably from its initial value. The velocity v has a small positive value, except for a short range of y near y_c where v reaches a maximum value, $v_{\max}$, of about 24 ft/sec. Through a series of calculations with different values of α we found that, as expected, $v_{\max}$ decreases with increasing resistance coefficient $|\alpha|$. However, we noted that the ratio of $v_{\max}(t)/v(0, t)$ *increases* with increasing $|\alpha|$.

b. Inflow of Cold Air from the North

Next we treated the case with the initial conditions (14)–(16), but with cold air coming in periodically from the north, that is,

$$v(Y, t) = V_p \left[\cos \frac{2\pi t}{T} - 1\right] \qquad t > 0. \tag{48}$$

The motion in $0 \leqslant y \leqslant Y$ is found to be stable for various values of the amplitude V_p and the period T considered.

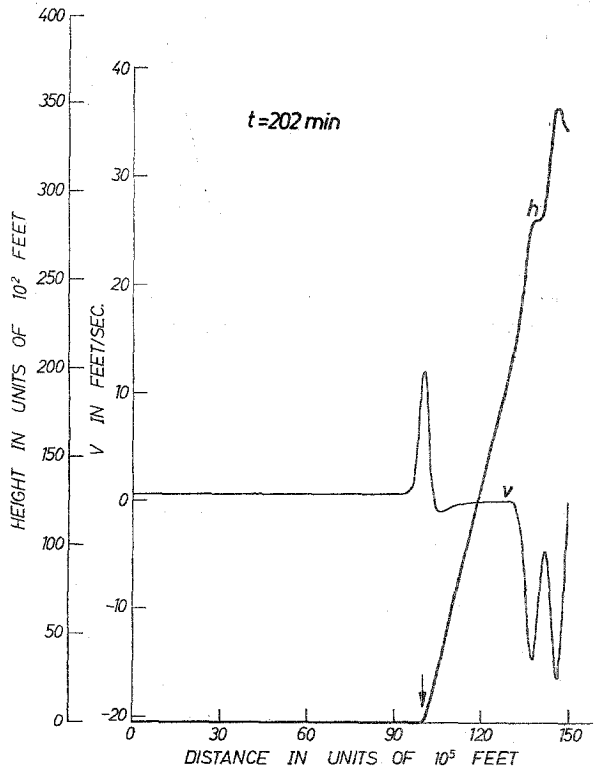

FIG. 10. Oscillatory inflow of cold air at north with period $T = 100$ min, amplitude $V_p = 10$ ft/sec. h and v after 202 minutes. The arrow indicates the initial location of the front.

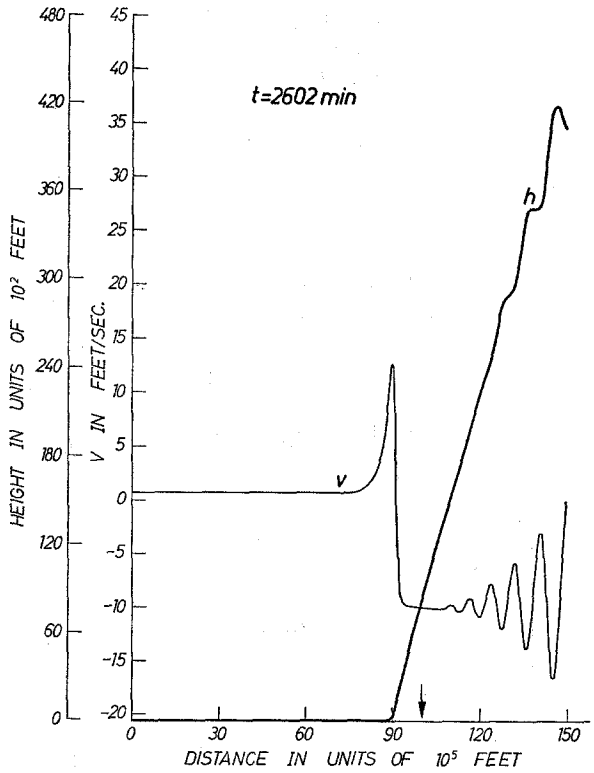

FIG. 11. Oscillatory inflow of cold air at north with period $T = 100$ min, amplitude $V_p = 10$ ft/sec. h and v after 2602 minutes. The arrow indicates the initial location of the front.

Figs. 10 and 11 show the motion in the case $V_p = 10$ ft/sec and $T = 100$ min. Fig. 10 exhibits the oscillations in height and velocity that have developed after 202 minutes. Fig. 11 shows that after 2602 minutes the front has moved to the south, and the maximum height has increased. The velocity oscillates around a negative mean value, owing to the net cold air flux coming in from the north. The disturbance wavelets propagate at an average velocity of about 170 ft/sec (which is in agreement with the "characteristic" speed), while the front moves at a rate of 6 ft/sec. The speed of propagation of the front is rather slow and will be discussed further subsequently.

Increasing the maximum velocity of cold air coming in at the north, increases the amplitude of oscillation, the growth of maximum height of the wedge, the speed

of propagation of the front and the average velocity in the cold air. Fig. 12 shows the results for $V_p = 50$ ft/sec, after 2002 minutes have elapsed.

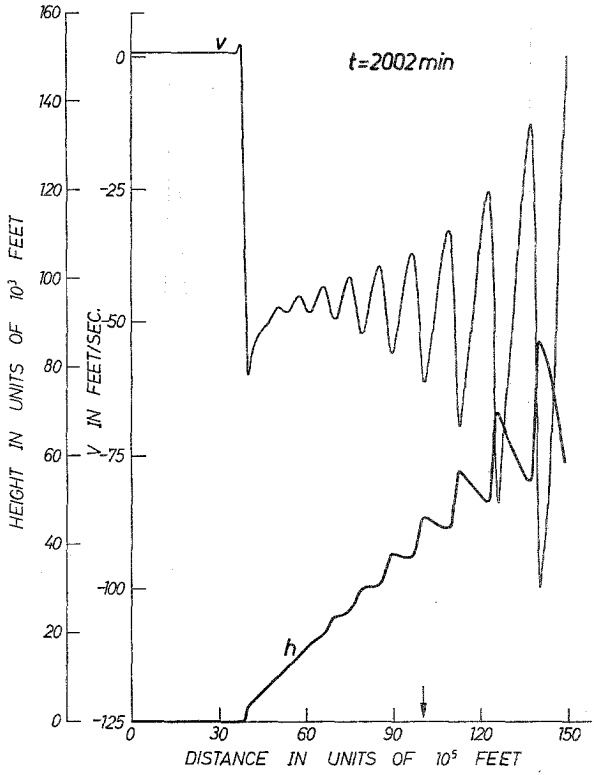

FIG. 12. Oscillatory inflow of cold air at north with period $T = 100$ min, amplitude $V_p = 50$ ft/sec. h and v after 2002 minutes. The arrow indicates the initial location of the front.

Upon decreasing the period of the cold air inflow to $T = 10$ min, we find that the velocity inside the cold wedge (except for a small interval at the north) does not follow the input velocity oscillations, and the depth of the wedge is found also to respond only slightly. Fig. 13 shows the result for $V_p = 10$ ft/sec, after 202 minutes. Fig. 14 shows the result for the larger velocity maximum, $V_p = 50$ ft/sec, after 2402 minutes. In the latter case the values of v and h are comparable to the mean values (over one oscillation) of the values of velocity and depth which arise from the inflow of longer period, shown in Fig. 12.

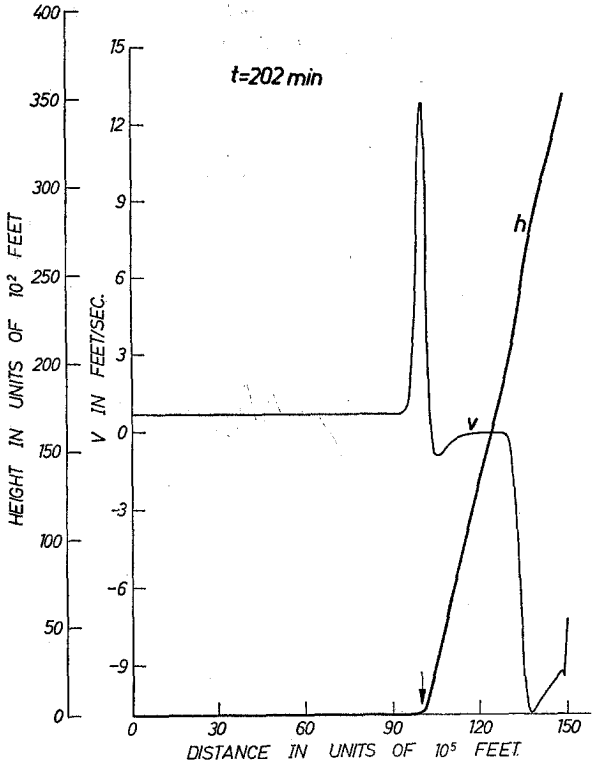

FIG. 13. Oscillatory inflow of cold air at north with period $T = 10$ min, amplitude $V_p = 10$ ft/sec. h and v after 202 minutes. The arrow indicates the initial location of the front.

Next, we consider a different time-variation of the inflow of cold air from the north, given by

$$v(Y, t) = \begin{cases} V_p \left[\cos \dfrac{2\pi t}{t} - 1\right] & 0 \leqslant t < \frac{1}{2}T \\ -2V_p & \frac{1}{2}T \leqslant t \end{cases} \tag{49}$$

i.e., a gradual increase in absolute value of velocity up to its maximum value $2V_p$, which is then maintained at this fixed rate. Results were for $V_p = 10$ and 50 ft/sec, and for $T = 100$, 10 and 1 minute. In all cases the front is found to gradually steepen and progress southward.

Figs. 15 and 16 are for $V_p = 10$ ft/sec, $T = 10$ min and $\alpha = -.001$. They show the velocity and height after 402 and 2402 minutes respectively. We notice the steepening of h in Fig. 15, in the vicinity of $y = 115$ units, which represents the

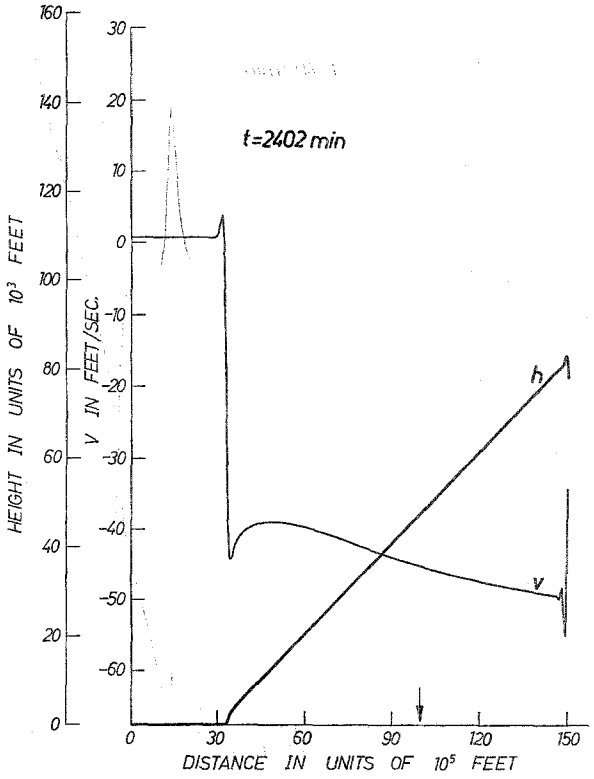

FIG. 14. Oscillatory inflow of cold air at north with period $T = 10$ min, amplitude $V_p = 50$ ft/sec. h and v after 2402 minutes. The arrow indicates the initial location of the front.

wave motion created by the build up of inflow from the north. In Fig. 16 the front has moved a greater distance than has the front in Fig. 11 (at a slightly later time). Clearly this difference is due to the fact that in Fig. 16 the steady inflow of cold air has velocity $-2V_p$, while for Fig. 11 the mean inflow velocity is only $-V_p$. For the very fast initial increase of velocity given by taking $T = 1$ min, we find that there is no appreciable difference in the resulting flow after 402 minutes. Prior to 402 minutes there is no noticeable irregularity due to the rapid increase of $v(Y, t)$.

9. Results for the Two Layer Model of Frontal Motion

The results were obtained by using the finite difference scheme (40)–(43) with the same constants as for the single layer model, except for Δt which had to be

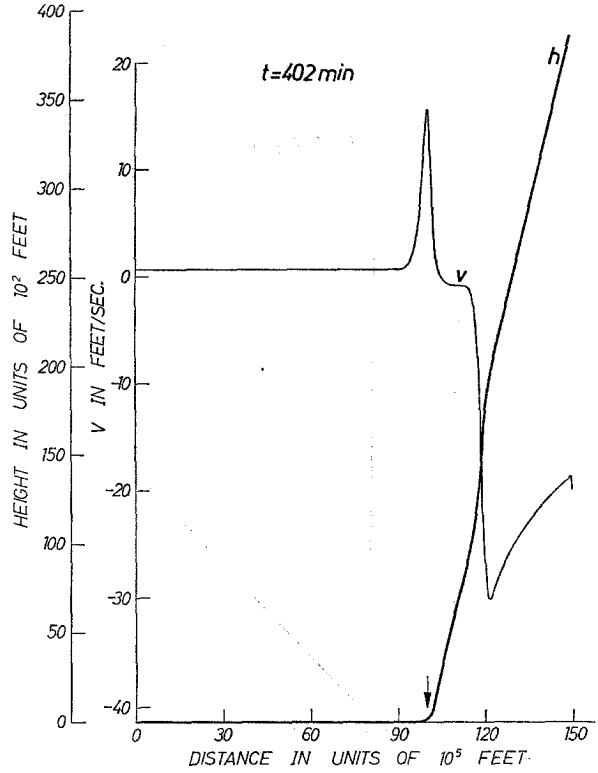

FIG. 15. Constant inflow of cold air, after the rise time $T/2$, with $T = 10$ min, amplitude $V_p = 10$ ft/sec. The arrow indicates the initial location of the front.

reduced in order to ensure numerical stability. We chose $\Delta t = 15$ sec so that $\lambda = \Delta t/\Delta s = .0003$ sec/ft. The height of the upper surface of the warm air at the north side was taken to be $h'(Y, 0) = 3h(Y, 0)$ at the initial time $t = 0$. That is, the total height of air at the north side was initially 3 times the maximum depth of the cold air layer. The total height is smallest at the north side and increases towards the south. The resistance coefficient is chosen in different cases to be in the range $-10^{-2} \leqslant \alpha \leqslant -10^{-6}$ and $h_c = .01$.

a. "STATIONARY" STATE

We considered first the "almost stationary" state given by (11)–(16) without any addition of cold air from the north. The differential equations with $\alpha = 0$ show that initially the flow is not in "equilibrium" only in the shallow cold layer. We would

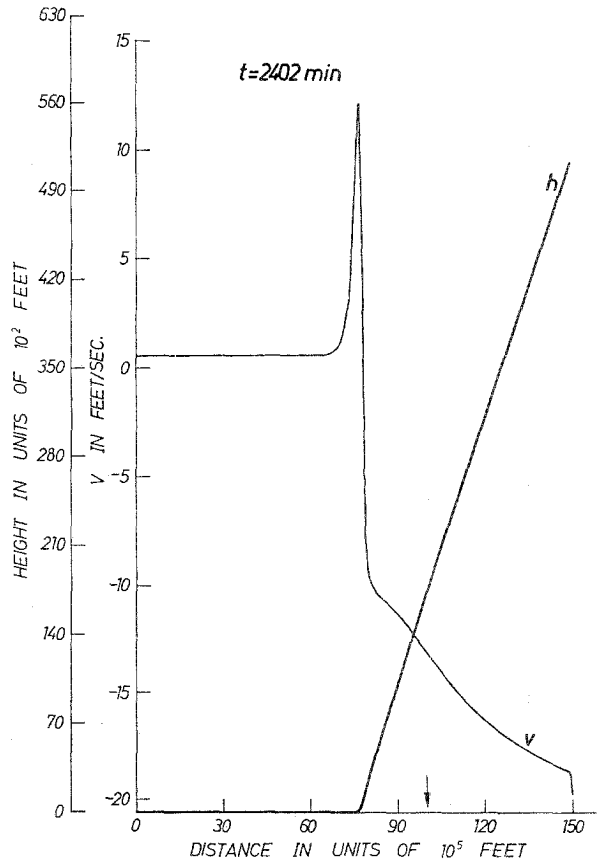

FIG. 16. Constant inflow of cold air, after the rise time $T/2$, with $T = 10$ min, amplitude $V_g = 10$ ft/sec. The arrow indicates the initial location of the front.

therefore expect very little motion to result. Fig. 17 shows the model after 1600 time-steps, i.e. after 400 minutes. The depth of cold air $h(y, t)$ is hardly changed from its initial value. Fig. 18 shows the total height $h'(y, t)$ and the velocity $w(y, t)$ in the warm air at about the same time. Here also h' is almost exactly at its initial value given by Eqs. (11)–(16). The velocity $w(y, t)$ has changed a bit from its initial value $w = 0$. In Fig. 17 we see that the velocity in the cold air layer is practically zero north of the front. Also we note that $v(y, t)$ is essentially zero onto the south of the front owing to the effect of the resistance term. It is only in the immediate vicinity of the front that the resistance term does not reduce the velocity to zero. The velocity curve is similar to the one in Fig. 9 for the single layer case. A

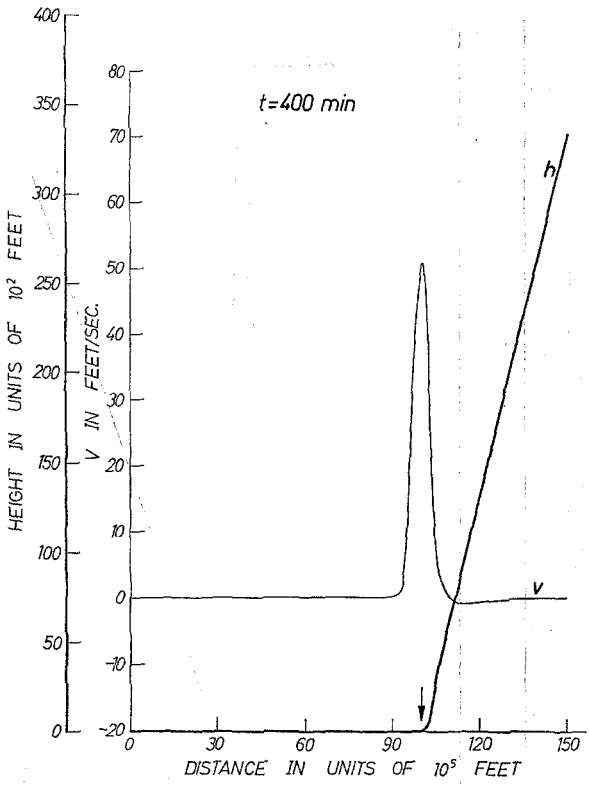

FIG. 17. Height h and velocity v of cold air for the "stationary" state in the two-layered model. The arrow indicates the initial location of the front.

comparison of the "stationary" states at different times and for various values of α, $-10^{-2} \leqslant \alpha \leqslant -10^{-6}$ and several values of $.01 \leqslant h_0 \leqslant .05h(Y, 0)$ shows that the variation of $v(y, t)$ between the single layer model and the two layer model is slight. The effect of varying the height of the warm air up to $h'(Y, 0) = 10h(Y, 0)$ is also slight in the present case of equilibrium initial and boundary conditions.

This simple case shows that the numerical procedure can be applied for a prolonged period. It is used in the next section for a study of the motion of the front when cold air comes in from the north side.

b. Inflow of Cold Air from the North

The boundary conditions of the problem are now changed so as to allow for a periodic variation of the velocity of the cold air, $v(Y, t)$, at the north. $v(Y, t)$ is given

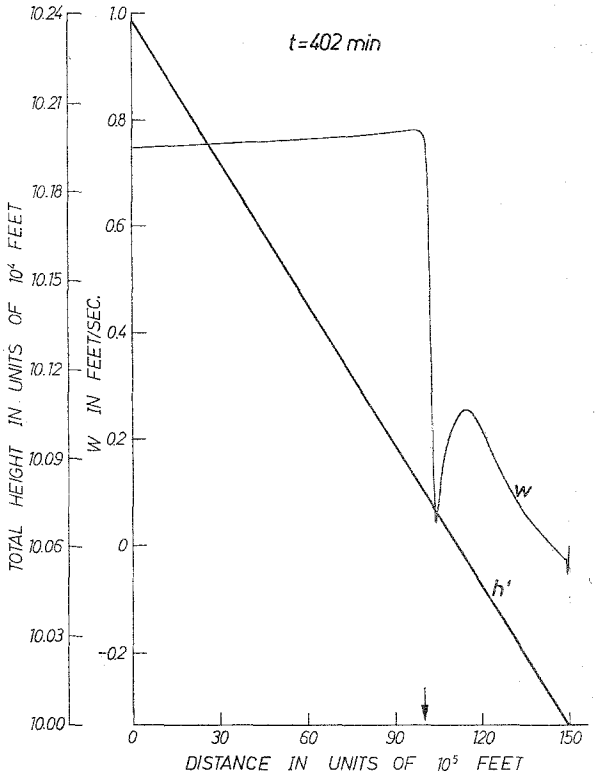

FIG. 18. Total height h' and velocity of warm air w, for the "stationary" state in the two-layered model. The arrow indicates the initial location of the front.

as in Eq. (48). Two kinds of boundary conditions for the velocity of the warm air, $w(Y, t)$, have been used:

(i) A "free" boundary condition in which w is obtained by linear extrapolation from values inside the region,

(ii) the condition of no flow,

$$w(Y, t) = 0, \qquad t > 0. \tag{50}$$

The difference in v, h, h' between the two cases is negligible. The warm air velocity $w(y, t)$ is smaller in magnitude throughout the region $y_c \leqslant y \leqslant Y$, when condition (50) is applied rather than the free condition.

Let us consider first the case when the period of oscillation is $T = 10$ min and the amplitude is given by $V_p = 10$ ft/sec. The constants in the equations are the

same as those used in the equilibrium case. Fig. 19 shows v and h after 12.5 minutes. The oscillations in velocity have propagated 15×10^5 feet, so that their phase velocity c is approximately 2000 ft/sec.

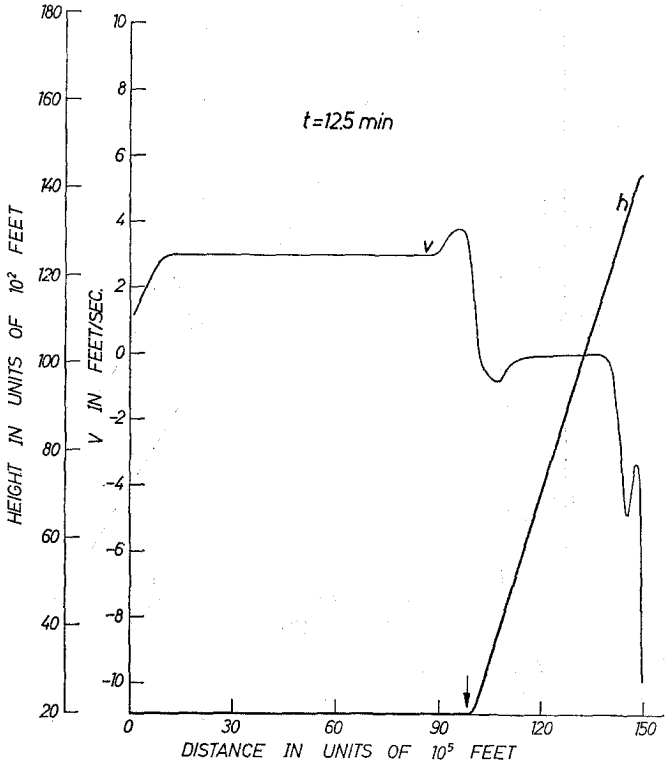

FIG. 19. Oscillatory inflow of cold air with period $T = 10$ min, amplitude $V_0 = 10$ ft/sec, in a two layer model. h and v after 12.5 minutes.

This value is larger than the speed of propagation of disturbances (called "sound speed") in the single layer model of the cold air, but is approximately the sound speed for a single fluid layer of depth about 30 km. In this calculation the initial maximum height of the cold air as given by (11)–(16) was $h(Y, 0) = h_m = 10$ km while $h'(Y, 0) = 30$ km, since the ratio of densities was $\rho'/\rho = 31.5521/32.1521$ (as assumed in Section 8). If the value of ρ'/ρ is decreased, we find that the maximum h_m at time $t = 0$ decreases and also the phase velocity, c, decreases. With all parameters as in Fig. 19, except that $\rho'/\rho = 30.1521/32.1521$, the phase velocity decreases to $c = 1333$ ft/sec and the height to $h_m = 4.6$ km.

Fig. 20 shows the results after 12.5 minutes, when $\rho'/\rho = 30.1521/32.1521$. For $\rho'/\rho = 29.1521/32.1521$ we find $c = 800$ ft/sec and $h_m = 2.2$ km.

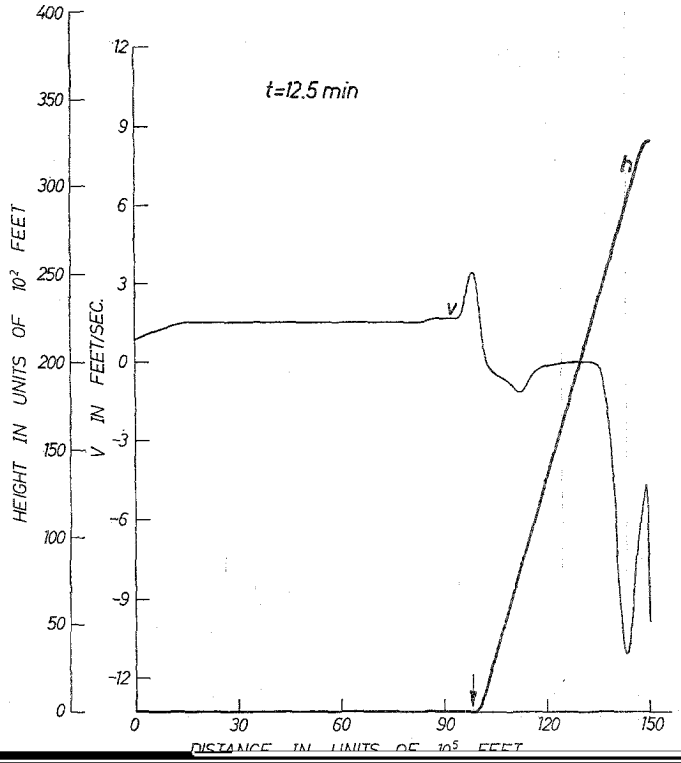

FIG. 20. Oscillatory inflow of cold air with period $T = 10$ min, amplitude $V_p = 10$ ft/sec, $\rho'/\rho = 30.1521/32.1521$, in a two layer model. h and v after 12.5 minutes.

When $\rho'/\rho = 31.5521/32.1521$ and the period of oscillation is $T = 10$ min, the velocity is seen to respond with oscillations. As seen in Fig. 13, for the corresponding single layer case, the cold air does not follow the oscillations of the inflow. But when the period of the inflow is decreased to $T = 1$ min, we find no oscillations are discernible in the velocity profile for the two layer case as well as the one layer case.

On the other hand, the curves $h(y, t)$ in Figs. 19 and 20 do not have any oscillations. This differs from the results for the single layer model, where we find oscillations in $h(y, t)$ (for fixed t) whenever oscillations in v (as a function of y) occur.

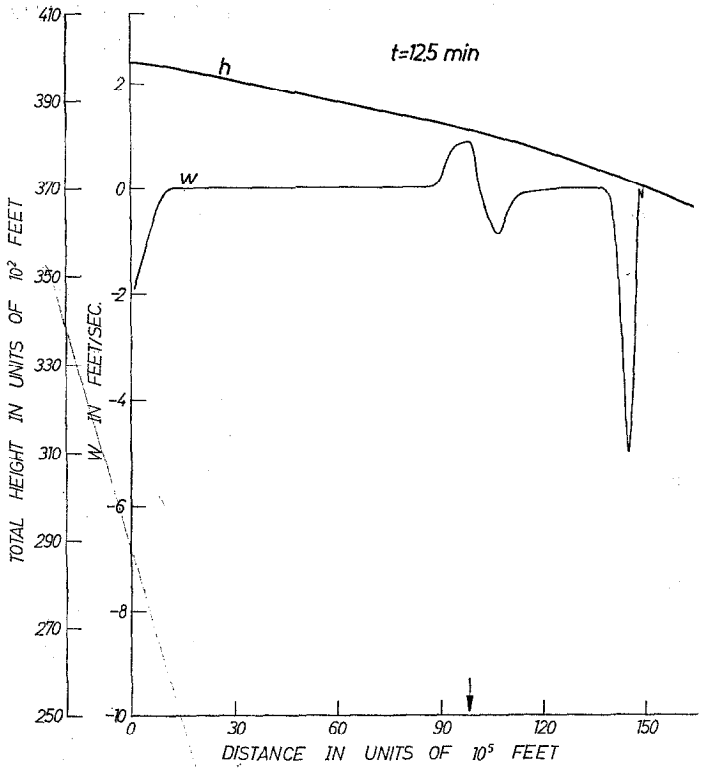

FIG. 21. Oscillatory inflow of cold air with period $T = 10$ min, amplitude $V_p = 10$ ft/sec, $\rho'/\rho = 30.1521/32.1521$, in a two layer model. h' and w after 12.5 minutes.

Fig. 21 for $\rho'/\rho = 30.1521/32.1521$ shows the effect on the upper layer of warm air: $w(y, t)$ oscillates while $h'(y, t)$, like $h(y, t)$, shows no oscillation and the slopes of h and h' stay essentially at their initial values. Fig. 22 shows v and h at a later time. Fig. 23, for $V_p = 50$ ft/sec, $T = 100$ min $\rho'/\rho = 31.5521/32.1521$ at time $t = 250$ min, shows oscillations both in v and in h. This behavior is similar to that seen in Fig. 10 for a single layer. Decreasing ρ'/ρ decreases the amplitude of oscillation at $y < Y$ after a prolonged time ($t > 100$ min) and the velocity distribution $v(y, t)$ comes closer to that of the corresponding single layer case.

We found that increasing the initial total height at the north, $H_T = h'(Y, 0)$, by a factor β, would increase the phase velocity of the oscillatory disturbance, c, by the factor $\sqrt{\beta}$.

The influence of varying the coefficient of resistance in the range $-10^{-2} \leqslant \alpha \leqslant -10^{-5}$ is negligible.

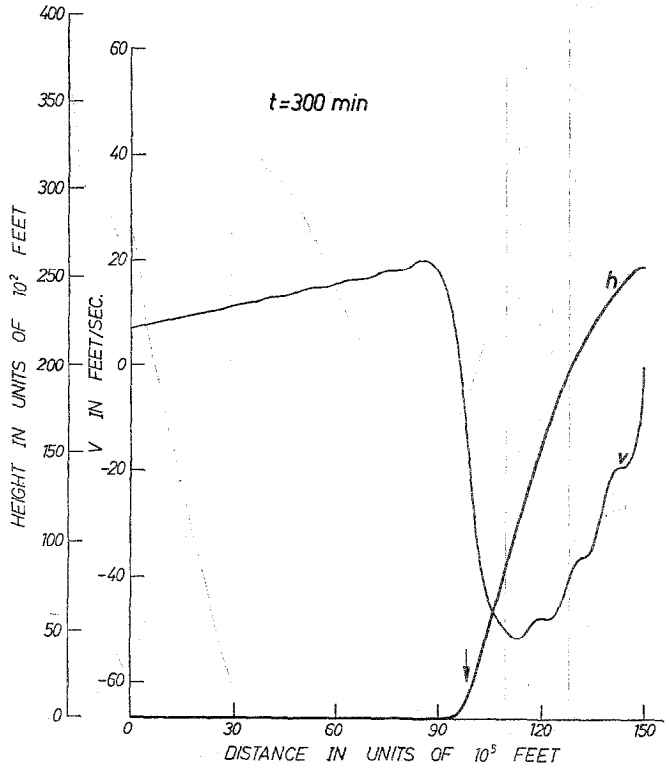

FIG. 22. Oscillatory inflow of cold air with period $T = 10$ min, amplitude $V_0 = 10$ ft/sec, in a two layer model. h and v after 300 minutes.

A comparison of results for several additional values of ρ', shows that decreasing the density ρ', decreases the speed of propagation c, and the velocity of the front.

In conclusion, we find that the two models differ in the effect of the oscillations on $h(y, t)$ and on the numerical values of c and of the velocity of the front. As a result, there is also a shift in the range of periods T of the input function $v(Y, t)$, for which $v(y, t)$ is an oscillatory function of y. Such differences in wave propagation properties of multilayered flow problems have been observed (e.g. see [9]).

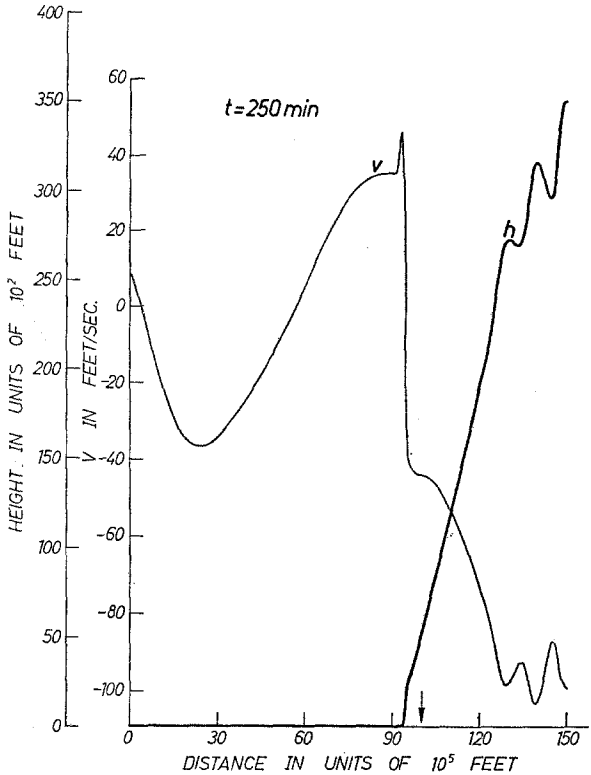

FIG. 23. Oscillatory inflow of cold air with period $T = 100$ min, amplitude $V_p = 50$ ft/sec, in a two layer model. h and v after 250 minutes.

REFERENCES

1. R. F. DRESSLER, Unsteady nonlinear waves in sloping channels. *Proc. Roy. Soc. London* **247A**, 186 (1958).
2. E. ISAACSON, Fluid dynamical calculations. *In* "Numerical Solution of Partial Differential Equations," pp. 35–49. Academic Press, New York (1966).
3. A. KASAHARA, E. ISAACSON, and J. J. STOKER, Numerical studies of frontal motion in the atmosphere—Tellus XVII, 3 (1965).
4. A. KASAHARA, E. ISAACSON, and J. J. STOKER, Numerical studies of frontal motion in the atmosphere—I, Report NYO-1480-6, New York University, New York (1964).
5. Y. MINTZ, Very long-term global integration of the primitive equations of atmospheric motion. World Meteorological Organization, Technical Note No. 66 (1965).
6. N. A. PHILLIPS, The general circulation of the atmosphere: a numerical experiment. *Quart. J. Roy. Meteorol. Soc.* **82**, 123–164 (1956).
7. J. J. STOKER, "Water waves." Wiley (Interscience), New York (1957).
8. G. B. WHITHAM, The effects of hydraulic resistance in the dam break problem. *Proc. Roy. Soc. London* **227A**, 399 (1954).
9. C. S. YIH, "Dynamics of nonhomogeneous fluids." Macmillan, New York (1965).